

Effect of layer sliding on the electronic and optical properties of corrugated silicene/indium selenide van der Waals heterostructure

M. W. YOUNIS^a, MASOOD YOUSAF^{b,*}, M. JUNAID IQBAL KHAN^c, JUNAID MUNIR^d, QURATUL AIN^e, TOHEED AKHTER^a

^aDepartment of Chemistry, University of Management and Technology, C-II, Johar Town, Lahore, 54770, Pakistan

^bDepartment of Physics, University of Education, Lahore, Pakistan

^cLaboratory of Theoretical and Experimental Physics, Department of Physics, Bahauddin Zakariya University, Multan, 60800, Pakistan

^dDepartment of physics, Riphah International University, Raiwind Road, Lahore, Pakistan

^eDepartment of Physics, University of Management and Technology, C-II, Johar Town, Lahore, 54770, Pakistan

Structural, electronic and optical properties of two dimensional corrugated silicene/InSe heterostructure have been calculated using density functional theory. The effect of layer sliding on the aforementioned physical properties is also studied. The maximum value of energy barrier along the sliding pathway is found to be 0.051 eV. To elucidate the electronic nature at the interface of the heterostructure, several interfacial properties have been discussed. Our employed strategy advocates that through layer sliding physical properties of a material can be tuned in a controlled manner.

(Received July 19, 2020; accepted June 11, 2021)

Keywords: Silicene, 2D indium selenide, vdW heterostructures, Tuning of properties, Layer sliding, Interfacial properties

1. Introduction

Efforts on the integration of two dimensional (2D) materials by creating van der Waals heterostructures (vdWHs) having exceptional properties is being emphasized by the research groups for the past few years [1-4]. Graphene [5] that has brought revolution in various scientific fields combines numerous exceptional properties such as high surface to mass ratio [6], excellent thermal [7] and electrical conductivity [5], and tremendous optical transparency [8]. However, zero band gap of graphene makes it unsuitable to be used as field effect transistors (FETs) in electronic industry [9]. To create some band gap in graphene, various ways were employed such as adsorption of hydrogen [10], reduction of size effect [11], functionalization [12], formation of heterostructures [2] etc. Researchers have devised ways to rectify intrinsic drawbacks and come out with novel 2D materials having versatile properties. 2D analogues of graphene such as hexagonal boron nitride (hBN), transition metal dichalcogenides (TMDCs, e.g., MoS₂), post-transition metal chalcogenide (e.g., InSe), phosphorene, silicene etc. have shown striking physical properties for efficient devices. The race is on the way to explore heterostructures based on newly discovered 2D materials with exceptional properties and methods to tune properties in a controlled manner.

Nowadays, formation of van der Waals heterostructures (vdWHs) is under great consideration and has become a creditable technique to tune the properties of

the 2D materials. In vdWHs, participating monolayers are positioned one over another and interact each other through van der Waals (vdW) forces harvesting some new physics at the interface. Heterostructure formation can induce extraordinary changes to the regular properties of the individual layers. For instance, hBN substrate enhances the electronic quality of graphene as compared with the pristine graphene [13]. Germanene/antimonene bilayer is found to have tunable electronic and optical properties with excellent visible light response, showing prospects for optoelectronic devices [14].

In this work, corrugated silicene and indium selenide (InSe) layers are selected to model silicene/InSe vdWHs. Recently prepared, group III-VI based 2D material InSe has depicted fascinating semiconducting properties such as direct band gap, high carrier mobility and charge density and odd p-type electronic behavior as compared with other 2D materials such as graphene, phosphorene and TMDCs [15]. Moreover, A few layers InSe based FETs has high on/off ratio up to 10⁸ and excellent electron carrier mobility [16]. Its wide band gap ranging from infrared to visible makes InSe a good photoresponsive material to be used as photodetectors [17]. Aforementioned excellent features of InSe endorse it to be a promising candidate for next generation high speed optoelectronics devices.

To discover novel set of properties, various heterostructures of InSe with other 2D materials have likewise been explored. For example, InSe/graphene vdWHs based photodetectors has four times more photoresponsivity than a single layer of InSe. Recently, it

is found that InSe/graphene vdWHs has a small band gap (5 meV) which makes it suitable for using in electronics and optoelectronics devices [18]. InSe/black phosphorus vdWHs has improved carrier mobility [19], better optical absorption, and efficient partitioning of photogenerated electron hole at the interface [20]. InSe/Arsenene vdWHs has high carrier mobility and direct band gap (0.876 eV) which can be further tuned by external electric field and strain [21]. The electronic properties of germanene/InSe vdWHs has been changed from indirect to direct band gap and from semiconductor to metallic state upon strain. Arsenene/InSe vdWHs has a direct band gap (563.7 meV) that can be utilized in various nanoelectronic fields [22]. In case of C₂N/InSe vdWHs, application of vertical strain along with electric field has revealed the switching of band structure from indirect to direct band gap [23].

Silicene is the other participating monolayer in our vdWHs having a zero band gap [24] and high Fermi velocity (10^6 ms⁻¹) [25]. As compared to graphene that contains sp² hybridized carbon atoms, silicene has sp³ hybridized silicon atoms with buckled hexagonal structure. Recently, various metallic substrates have been tried to synthesize silicene experimentally [26]. However, the strong interaction between silicene and substrates results in the mixing of electronic states causing semimetal to metal transition. This problem needs to be overcome in order to use silicene in electronic devices that require an opened band gap at the Dirac point along with higher charge mobility. Various tailoring techniques such as fluorination [27], hydrogenation [28] and application of electric field [29] have been tried to successfully open the band gap at Fermi level. Silicene has been set over various semiconducting honeycomb substrates to open its band gap [30, 31]. For example, recently, Sattar *et al* [32], Zhang *et. al.* [33] and Le *et.al.* [24] opened the band gap of 0.023 eV, 0.997 eV and 0.0197 eV at the Dirac point of silicene when silicene is in combination with hBN, gallium phosphide (GaP) and gallium selenide (GaSe), respectively. This opening of band gap induces semiconducting character in silicene, making it suitable material for optoelectronics and strain sensors.

2. Computational method

Density functional theory (DFT) supported Quantum ESPRESSO (QE) code [34], which employs pseudopotentials and plane wave basis sets, is used to execute all calculations provided in the manuscript. The exchange and correlation energy is calculated using the Perdew and Wang type functional [35]. Norm-conserving

type pseudopotentials [36] Si.pw-mt_fhi.UPF, In.pw-mt_fhi.UPF and Se.pw-mt_fhi.UPF produced by Martins-Troullier method [37], are used for computing atomic potentials of participating atoms i.e., Si, In and Se, respectively. Cut-off energies of 80 Ry and 320 Ry are selected, more than sufficient to describe the plane wave basis set for wave function and charge density, respectively. Brillouin zone integration with $7 \times 7 \times 1$ K points is performed and a larger vacuum spacing ($>10 \text{ \AA}$) is set in the supercell to avoid any possible electronic interactions resulted from repeated copies of the supercell in periodic codes such as QE. The nudged elastic band (NEB) method [38, 39] as implemented in the QE code is utilized to find out the minimum energy pathway with transition energies.

3. Results and discussion

3.1. Structural properties

First of all, in order to model a 2D heterostructure that can fulfill the needs for cutting-edge devices such as withstanding external effect [40], ease of device fabrication [41] etc., we cleverly selected layer of InSe and silicene to form silicene/InSe heterostructure. Selection of silicene and InSe as participating monolayers is advantageous because of the smaller difference of lattice constants (a) between silicene (3.862 Å) and InSe (3.860 Å), which give rise to a negligible (0.07%) lattice mismatch. Recently reported lattice mismatch for silicene/InSe heterostructure is 0.5% [31], which is in close agreement with our calculated value. The better in plane lattice constant compatibility of silicene makes it suitable stacking candidate for InSe substrate.

Silicene/InSe heterostructure can be formed by placing silicene over InSe layer in number of possible ways as shown in Fig. 1. For convenience, from here on, silicon (Si) atoms found in the upper and lower plane of silicene's buckled structure will be referred as up-Si and down-Si atoms, respectively. Buckling parameter, which is the distance between upper plane Si atoms and lower plane Si atoms is calculated to be 0.42 Å. Whereas, thickness of InSe layer (d) is calculated as the distance between top and bottom most selenium (Se) atoms that form corrugation at both sides of InSe. The interlayer distance, which is the distance between the lower plane Si-atoms of buckled silicene and top most Se atoms of InSe, is found to be 2.92 Å. Calculated lattice constant (a) of participating monolayers, buckling parameter of silicene (Δz), thickness of InSe and the vdW gap in the heterostructure are given in the Table 1.

Table 1. Calculated lattice constant (a), buckling parameter for silicene (Δz), thickness of InSe (d) and vdW gap of the most stable heterostructure

2D Materials	a (Å)		Δz (Å)		d (Å)	vdW gap (Å)	
Silicene	3.862	3.868 [31]	0.423	---	---	---	---
InSe	3.860	3.95 [31]	---	---	5.70	---	---
Silicene/InSe heterostructure	3.877	3.886 [31]	0.439	0.465 [31]	5.33	2.923	2.933 [31]

3.2 Stability and layer sliding

To find the most stable layout of silicene over InSe monolayer, different stacking patterns of silicene over InSe have been identified. Subfigures showing side [(a), (c), (e), and (g)] and top [(b), (d), (f), and (h)] views of the optimized geometries of possible stacking patterns are part of figure 1. The most stable stacking pattern is obtained [figure 1(c)/(d)] by comparing total energies of the possible configurations. The configuration 1(a)/(b) differs only slightly in energy by 0.04 eV whereas the other configurations 1(e)/(f) and 1(g)/(h) have significantly higher energy by 0.26 eV and 0.31 eV, respectively, than the energy calculated for the most stable configuration 1(c)/(d). In case of the most optimum configuration (1(c)/(d)), up-Si atoms are positioned directly above the indium atoms whereas configuration shown in 1(a)/(b) has down-Si atoms on indium atoms. For least stable configurations given in subfigures 1(e)/(f) and 1(g)/(h) has

down-Si and up-Si atoms on selenium atoms, respectively. For the most stable stacking pattern [Fig. 1(c)/(d)], silicene is slid over InSe layer. Sliding path is equal to the bond length ($L = 2.27 \text{ \AA}$) between the silicon atoms in silicene/InSe heterostructure. The sliding of silicene is carried out in ten equal parts (one part = $L/10$), and the total energy of the heterostructure is collected after each portion of sliding and is compared with the total energy of the most stable heterostructure. Relative total energy is plotted against percentage sliding pathway and is presented as subfigure 1(i). Representative side/top view of configurations of heterostructures appearing at the start [subfigure 1(c)/(d)], middle [subfigure 1(j)/(k)] and end [subfigure 1(l)/(m)] of the sliding pathway are shown in Fig. 1. Direction of sliding is indicated by red arrows as shown in the subfigures 1(k) and 1(m) of Fig. 1.

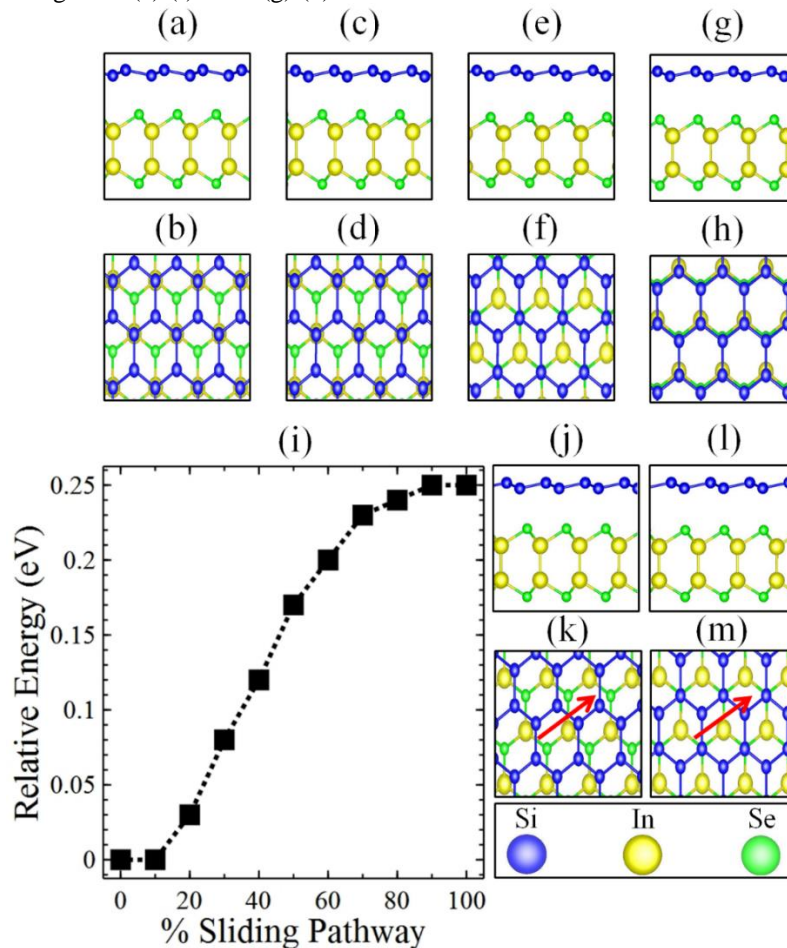


Fig. 1. Side [subfigures (a), (c), (e) and (g)] and top [subfigures (b), (d), (f) and (h)] views of heterostructures showing possible stacking patterns of buckled silicene over InSe monolayer. The most stable configuration is shown as subfigure (c)/(d). The change in total energy due to sliding of silicene over InSe layer is provided in panel (i). The subfigures (j)/(k) and (l)/(m) represent the side/top view of the heterostructure on covering half and full length of the sliding pathway, respectively. Direction of sliding is indicated by arrows in red colour (color online)

During the course of sliding, calculated change in van der Waals (vdW) gap between the contributing layers of the heterostructure is shown in the Fig. 2. VdW gap

increases as silicene slides over InSe. VdW gap follow a similar trend to that of change in total energy along the sliding pathway. For understudy system, the decrease in

vdW forces results in the increase of total energy of the system.

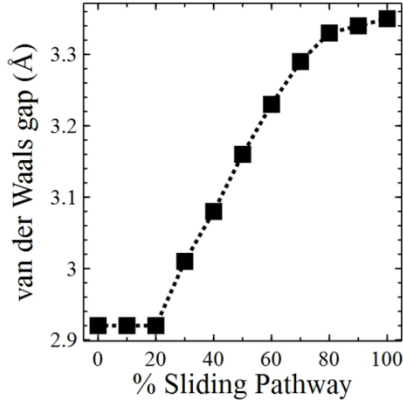


Fig. 2. Variation of van der Waals gap as due to sliding of silicene over InSe layer

Potential energy scans along the sliding pathway are also investigated, and the energy barrier (E_b) between two consecutive divisions of the pathway is calculated using nudged elastic band (NEB) method. Values of E_b obtained along the sliding pathway are presented in Fig. 3. Each value of E_b corresponds to two consecutive divisions of the sliding pathway from 0% to 10%, 10% to 20%, 20% to 30%, 30% to 40%, 40% to 50%, 50% to 60%, 60% to 70%, 70% to 80%, 80% to 90% and 90% to 100%. Uppercased letter A, B, C, D, E, F, G, H, I and J are marked for aforementioned path intervals, respectively. The plot demonstrates that E_b values first increase to the maximum value of 50.77 meV (when sliding from 30% to

40%) and then gradually decrease on further completion of the sliding.

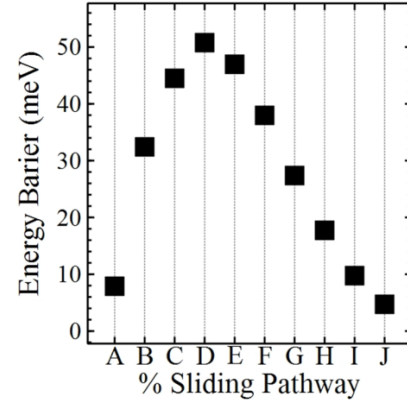


Fig. 3. Calculated sliding energy barrier for silicene/InSe heterostructure. Energy barrier values are calculated for consecutive divisions of the sliding pathway from 0% to 10%, 10% to 20%, 20% to 30%, 30% to 40%, 40% to 50%, 50% to 60%, 60% to 70%, 70% to 80%, 80% to 90% and 90% to 100%, which are marked by uppercase letters A, B, C, D, E, F, G, H, I and J, respectively

3.3. The dielectric functions

Optical properties relating to silicene/InSe heterostructure are also investigated with the help of complex dielectric function, $\epsilon(\omega) = \epsilon_1(\omega) + i\epsilon_2(\omega)$. Imaginary part ($\epsilon_2(\omega)$) of the complex dielectric function that can be related to polarization losses of the material in alternating fields and can be calculated as follow [42],

$$\epsilon_2(\omega) = \frac{4\pi^2 e^2}{\Omega} \lim_{q \rightarrow 0} 1/q^2 \sum_{c,v,k} 2\omega_k \delta(\epsilon_{ck} - \epsilon_{vk} - \omega) \times \langle u_{ck} + e_{\alpha q} | u_{vk} \rangle \langle u_{ck} + e_{\beta q} | u_{vk} \rangle^* \quad (1)$$

While, the real part ($\epsilon_1(\omega)$) of dielectric function can be obtained by using the Kramers-Kroing relation,

$$\epsilon_1(\omega) = 1 + \frac{2}{\pi} P \int_0^\infty \frac{\epsilon_2^{\alpha\beta}(\omega') \omega'}{\omega'^2 - \omega^2 + i\eta} d\omega' \quad (2)$$

The calculated in-plane and out-of-plane dielectric function of different silicene/InSe vdWHs is shown in the Fig. 4. The plots relating to unslided heterostructure [subfigures (a)] and on coverage of half [subfigures (b)] and full length [subfigures (c)] of the sliding pathway show an identical trend with small differences. Before, midway and after complete sliding of silicene, there are

multiple response peaks under 4.5 eV with one significant peak around 0.5 eV. The in-plane dielectric function after reaching maximum value around 0.5 eV in all subfigures varies throughout with small magnitude. It is clear from the calculations that there exists a major difference between the dielectric functions along the planar and vertical direction.

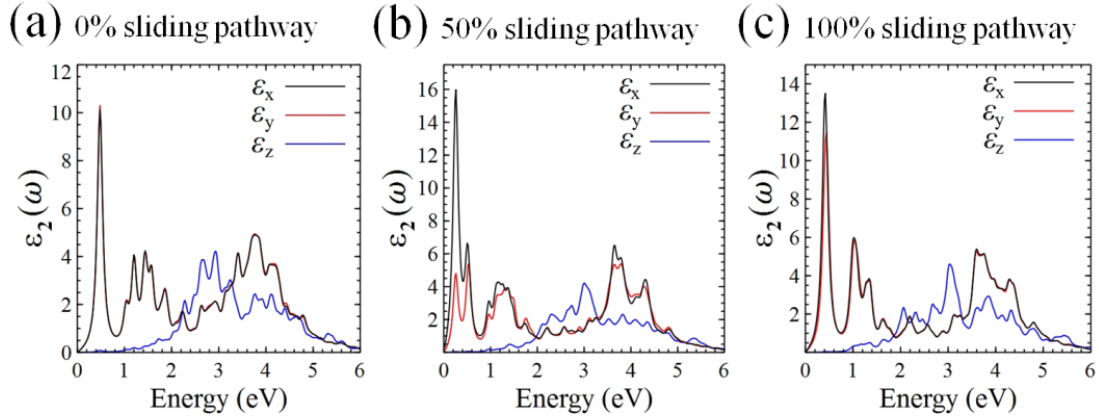


Fig. 4. Calculated in-plane (ϵ_x and ϵ_y) and out-of-plane (ϵ_z) dielectric function for silicene/InSe heterostructure (color online)

3.4. Interfacial electronic properties

The calculated values for interfacial electronic properties such as the planar average charge density difference ($\Delta\rho$), dipole charge transfer (ΔQ) and interface dipole moment ($\Delta\mu$) of 2D silicene/InSe heterostructure are investigated and are part of Figs. 5, 6 and 7, respectively. All aforementioned calculated values as a function of the vertical length of the supercell are given for unslided heterostructure [subfigures 5(a), 6(a) and 7(a)] and on coverage of half [subfigures 5(b), 6(b) and 7(b)] and full length [subfigures 5(c), 6(c) and 7(c)] of the sliding pathway. Vertical red and blue dashed lines in all the subfigures of Figs. 5, 6 and 7 represent the position of InSe and silicene monolayers, respectively.

Among the first interfacial electronic property, the planar average charge density difference ($\Delta\rho$), can be calculated as

$$\Delta\rho(z) = \rho(z)_{\text{silicene}} - \rho(z)_{\text{InSe}} \quad (3)$$

where $\rho(z)_{\text{silicene/InSe}}$, $\rho(z)_{\text{silicene}}$ and $\rho(z)_{\text{InSe}}$ are the planar average charge densities relating to silicene/InSe heterostructure, silicene and InSe monolayer, respectively. The planar surface (x-y plane) of the supercell is integrated to obtain the value of the aforesaid densities. The average charge density difference ($\Delta\rho$) is available along z-axis, and its negative and positive values are related to the depletion and accumulation of electron density in the heterostructure.

$$\rho(z) = \int \rho(x, y, z) dx dy \quad (4)$$

Before sliding, it can be seen from subfigure 5(a) that $\rho(z)$ slightly decreases near InSe and then increases while near silicene layer it decreases sharply. For 50% [figure 6 (b)] and 100% [figure 6 (c)] coverage of sliding pathway by silicene, charge density fluctuates between the two layers with larger value at the center of two layers

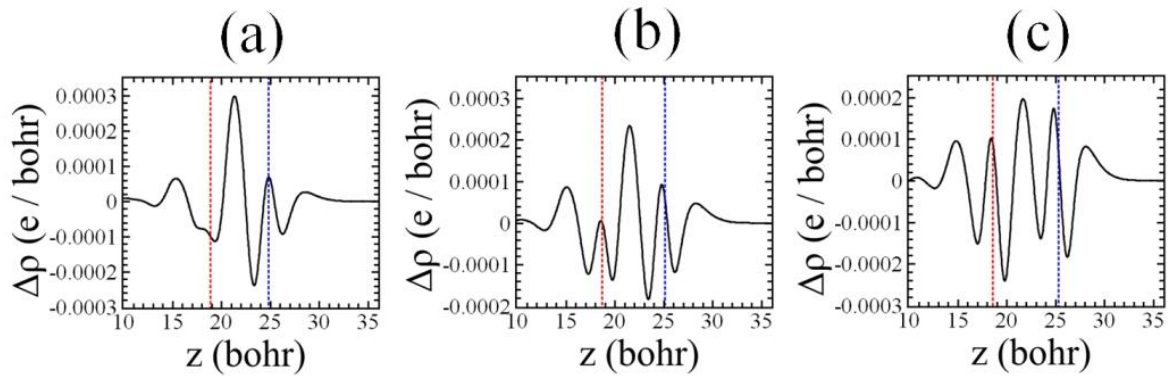


Fig. 5. Calculated planar average charge density ($\Delta\rho$) for initial, halfway and final stage of the layer sliding as shown in subfigure (a), (b) and (c), respectively. $\Delta\rho$ is calculated as a function of vertical distance along z-axis of the supercell (color online)

Furthermore, $\rho(z)$ can be utilize to calculate the ΔQ and μ by following equations;

$$\Delta Q(z) = \int \Delta\rho(z) dz \quad (5)$$

$$\mu(z) = \int z\Delta\rho(z)dz \quad (6)$$

As defined by equation 4, ΔQ describe the direction of charge transfer between participating layers. The negative values of ΔQ are related to the charge transfer from InSe to silicene. The positive values of ΔQ near silicene

subfigure 6(a), indicate the charge transfer from silicene to InSe. At midway sliding pathway [Fig. 6(b)], there is a small increase in the positive values near silicene while on completion of sliding pathway [Fig. 6(c)], transference of the charge takes place from InSe to silicene.

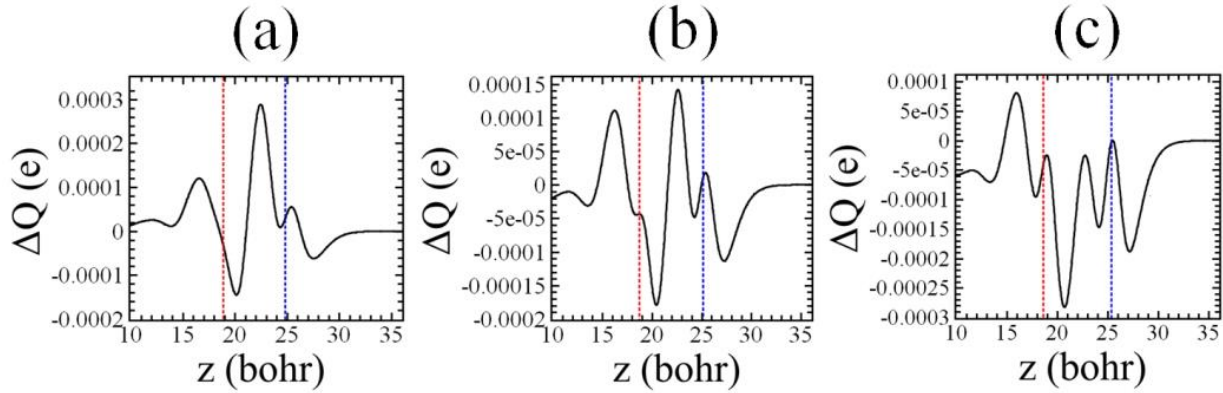


Fig. 6. Calculated charge transference (ΔQ) for initial, halfway and final stage of the layer sliding as shown in subfigure (a), (b) and (c), respectively (color online)

Another interfacial electronic property $\mu(z)$ is obtained with the help of integration along the vertical length (z -axis) of the supercell as defined by equation 5. Hump of positive values of $\mu(z)$ in all the subfigures of

Fig. 7 keep on decreasing near silicene layer. Also, it can be noted from Fig. 6 and Fig. 7, both ΔQ and $\mu(z)$ follow similar and the difference lies in magnitude of aforementioned quantities.

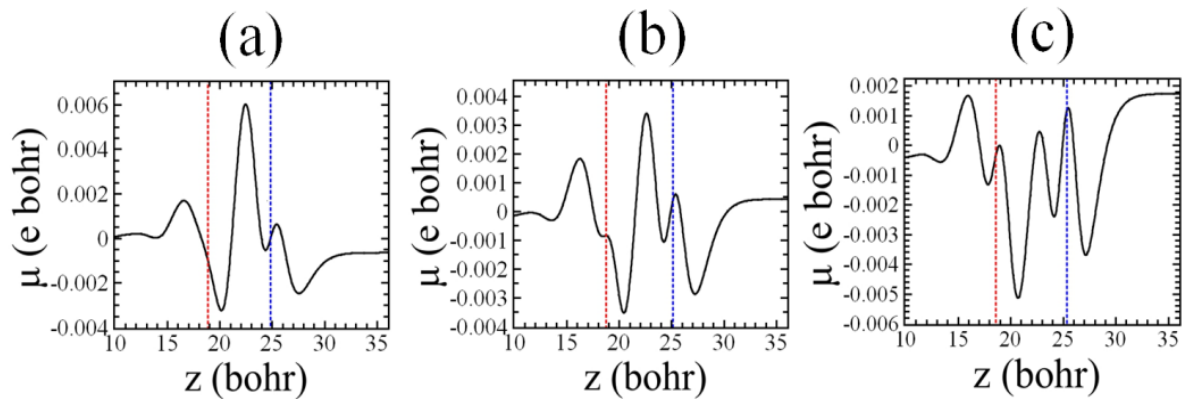


Fig. 7. Calculated interface dipole moment (μ) for initial, halfway and final stage of the layer sliding as shown in subfigure (a), (b) and (c), respectively (color online)

4. Conclusion

First-principles calculations are carried out to investigate structural, electronic and optical properties of two dimensional silicene/InSe van der Waals heterostructures (vdWHs). In order to vary aforementioned physical properties, one layer of the vdWHs is slid over another and total energy is also collected after each portion of the sliding pathway. Potential energy scans along the course of sliding pathway reveal that the maximum energy

barrier is found to be 0.051 eV for sliding of silicene over InSe layer. Furthermore, interfacial planar average charge density difference, charge transfer and dipole moment for silicene/InSe heterostructure are calculated. Along the sliding pathway, the maximum and minimum value of average charge density difference are found near InSe and silicene layer, respectively. The employed method opens the possibility of obtaining custom-tailored properties in layer materials.

References

- [1] K. Ren, J. Yu, W. Tang, *J. Alloys Compd.* **812**, 152049 (2020).
- [2] K. Si, J. Ma, C. Lu, Y. Zhou, C. He, D. Yang, X. Wang, X. Xu, *Appl. Surf. Sci.* **507**, 145082 (2020).
- [3] K. Ren, M. Sun, Y. Luo, S. Wang, J. Yu, W. Tang, *Appl. Surf. Sci.* **476**, 70 (2019).
- [4] W.-Z. Xiao, L. Xu, Q.-Y. Rong, X.-Y. Dai, C.-P. Cheng, L.-L. Wang, *Appl. Surf. Sci.* **504**, 144425 (2020).
- [5] K. S. Novoselov, A. K. Geim, S. V. Morozov, D. Jiang, Y. Zhang, S. V. Dubonos, I. V. Grigorieva, A. A. Firsov, *Science* **306** (5696), 666 (2004).
- [6] M. D. Stoller, S. Park, Y. Zhu, J. An, R. S. Ruoff, *Nano letters* **8**(10), 3498 (2008).
- [7] A. A. Balandin, S. Ghosh, W. Bao, I. Calizo, D. Teweldebrhan, F. Miao, C. N. Lau, *Nano Letters* **8**(3), 902 (2008).
- [8] R. R. Nair, P. Blake, A. N. Grigorenko, K. S. Novoselov, T. J. Booth, T. Stauber, N. M. Peres, A. K. Geim, *Science* **320**(5881), 1308 (2008).
- [9] F. Schwierz, *Nat. Nanotechnol.* **5**(7), 487 (2010).
- [10] R. Balog, B. Jørgensen, L. Nilsson, M. Andersen, E. Rienks, M. Bianchi, M. Fanetti, E. Lægsgaard, A. Baraldi, S. Lizzit, *Nat. Mater.* **9**(4), 315 (2010).
- [11] M. Y. Han, B. Özyilmaz, Y. Zhang, P. Kim, *Phys. Rev. Lett.* **98**(20), 206805 (2007).
- [12] Q. Tang, Z. Zhou, Z. Chen, *Nanoscale* **5**(11), 4541 (2013).
- [13] C. R. Dean, A. F. Young, I. Meric, C. Lee, L. Wang, S. Sorgenfrei, K. Watanabe, T. Taniguchi, P. Kim, K. L. Shepard, *Nat. Nanotechnol.* **5**(10), 722 (2010).
- [14] X. Chen, Q. Yang, R. Meng, J. Jiang, Q. Liang, C. Tan, X. Sun, *J. Mater. Chem. C* **4**(23), 5434 (2016).
- [15] K. Xu, L. Yin, Y. Huang, T. A. Shifa, J. Chu, F. Wang, R. Cheng, Z. Wang, J. He, *Nanoscale* **8**(38), 16802 (2016).
- [16] D. Boukhvalov, B. Gürbulak, S. Duman, L. Wang, A. Politano, L. Caputi, G. Chiarello, A. Cupolillo, *Nanomaterials* **7**(11), 372 (2017).
- [17] S. R. Tamalampudi, Y.-Y. Lu, U. R. Kumar, R. Sankar, C.-D. Liao, B. K. Moorthy, C.-H. Cheng, F. C. Chou, Y.-T. Chen, *Nano letters* **14**(5), 2800 (2014).
- [18] K. D. Pham, N. N. Hieu, V. V. Ilyasov, H. V. Phuc, B. D. Hoi, E. Feddi, N. V. Thuan, C. V. Nguyen, *Superlattices and Microstructures* **122**, 570 (2018).
- [19] Y.-M. Ding, J.-J. Shi, C. Xia, M. Zhang, J. Du, P. Huang, M. Wu, H. Wang, Y.-L. Cen, S.-H. Pan, *Nanoscale* **9**(38), 14682 (2017).
- [20] X. Niu, Y. Li, Y. Zhang, Q. Zheng, J. Zhao, J. Wang, *J. Mater. Chem. C* (2019).
- [21] Z. Xie, F. Sun, R. Yao, Y. Zhang, Y. Zhang, Z. Zhang, J. Fan, L. Ni, L. Duan, *Appl. Surf. Sci.* **475**, 839 (2019).
- [22] N. Song, H. Ling, Y. Wang, L. Zhang, Y. Yang, Y. Jia, *J. Solid State Chem.* **269**, 513 (2019).
- [23] K. D. Pham, N. N. Hieu, L. M. Bui, H. V. Phuc, B. D. Hoi, L. T. Tu, L. G. Bach, V. V. Ilyasov, B. Amin, M. Idrees, *Chem. Phys. Lett.* **716**, 155 (2019).
- [24] P. Le, N. N. Hieu, L. M. Bui, H. V. Phuc, B. D. Hoi, B. Amin, C. V. Nguyen, *Phys. Chem. Chem. Phys.* **20**(44), 27856 (2018).
- [25] S. Cahangirov, M. Topsakal, E. Aktürk, H. Şahin, S. Ciraci, *Phys. Rev. Lett.* **102**(23), 236804 (2009).
- [26] C. Lin, C.-L. Lin, R. Arafune, K. Kawahara, M. Kanno, N. Tsukahara, E. Minamitani, Y. Kim, M. Kawai, N. Takagi, *Phys. Rev. Lett.* **110**, 076801 (2013).
- [27] Y. Ding, Y. Wang, *Appl. Phys. Lett.* **100**(8), 083102 (2012).
- [28] T. H. Osborn, A. A. Farajian, O. V. Pupyshva, R. S. Aga, L. L. Y. Voon, *Chem. Phys. Lett.* **511**(1-3), 101 (2011).
- [29] N. Drummond, V. Zolyomi, V. Falko, *Phys. Rev. B* **85**(7), 075423 (2012).
- [30] Y. Ding, Y. Wang, *Appl. Phys. Lett.* **103**(4), 043114 (2013).
- [31] Y. Fan, X. Liu, J. Wang, H. Ai, M. Zhao, *Phys. Chem. Chem. Phys.* **20**(16), 11369 (2018).
- [32] S. Sattar, Y. Zhang, U. Schwingenschlögl, *Adv. Theory. Simul.* **1**(11), 1800083 (2018).
- [33] P. Zhang, X. Yang, W. Wu, L. Tian, H. Cui, K. Zheng, J. Jiang, X. Chen, H. Ye, *Chem. Phys. Lett.* **700**, 114 (2018).
- [34] P. Giannozzi, S. Baroni, N. Bonini, M. Calandra, T. Car, C. Cavazzoni, D. Ceresoli, G. L. Chiarotti, M. Cococcioni, I. Dabo, *J. Phys.-Condens. Mat.* **21**(39), 395502 (2009).
- [35] J. P. Perdew, Y. Wang, *Phys. Rev. B* **45**(23), 13244 (1992).
- [36] M. Schlüter, D. Hamann, C. Chiang, *Phys. Rev. Lett.* **43**, 1494 (1979).
- [37] N. Trouiller, J. L. Martins, *Phys. Rev. B* **43**(3), 1993 (1991).
- [38] G. Henkelman, H. Jónsson, *J. Chem. Phys.* **111**(15), 7010 (1999).
- [39] E. Weinan, W. Ren, E. Vanden-Eijnden, *Phys. Rev. B* **66**(5), 052301 (2002).
- [40] G. Li, L. Zhang, W. Xu, J. Pan, S. Song, Y. Zhang, H. Zhou, Y. Wang, L. Bao, Y. Y. Zhang, *Adv. Mater.* **30**(49), 1804650 (2018).
- [41] D. T. Larson, I. Fampiou, G. Kim, E. Kaxiras, *J. Phys. Chem. C* **122**(43), 24535 (2018).
- [42] B. Qiu, X. Zhao, G. Hu, W. Yue, J. Ren, X. Yuan, *Nanomaterials* **8**(11), 962 (2018).

*Corresponding author:masood.yousaf@ue.edu.pk